JACS
JOURNAL OF THE AMERICAN CHEMICAL SOCIETY
pubs.acs.org/JACS
Article

A Small Molecule Strategy for Targeting Cancer Stem Cells in Hypoxic Microenvironments and Preventing Tumorigenesis

Ji Hyeon Kim, Peter Verwilst, Miae Won, Junhyoung Lee, Jonathan L. Sessler,* Jiyou Han,* and Jong Seung Kim*

Cite This: https://doi.org/10.1021/jacs.1c03875 Read Online

ACCESS | Metrics & More | Article Recommendations | Supporting Information

ABSTRACT: Breast cancer consists of heterogenic subpopulations, which determine the prognosis and response to chemotherapy. Among these subpopulations, a very limited number of cancer cells are particularly problematic. These cells, known as breast cancer stem cells (BCSCs), are thought responsible for metastasis and recurrence. They are thus major contributor to the unfavorable outcomes seen for many breast cancer patients. BCSCs are more prevalent in the hypoxic niche. This is an oxygen-deprived environment that is considered crucial to their proliferation, stemness, and self-renewal but also one that makes BCSCs highly refractory to traditional chemotherapeutic regimens. Here we report a small molecule construct, **AzCDF**, that allows the therapeutic targeting of BCSCs and which is effective in normally refractory hypoxic tumor environments. A related system, **AzNap**, has been developed that permits CSC imaging. Several design elements are incorporated into **AzCDF**, including the CAIX inhibitor acetazolamide (Az) to promote localization in MDA-MB-231 CSCs, a dimethylnitrothiophene subunit as a hypoxia trigger, and a 3,4-difluorobenzylidene curcumin (CDF) as a readily released therapeutic payload. This allows **AzCDF** to serve as a hypoxia-liable molecular platform that targets BCSCs selectively which decreases CSC migration, retards tumor growth, and lowers tumorigenesis rates as evidenced by a combination of in vitro and in vivo studies. To the best of our knowledge, this is the first time a CSC-targeting small molecule has been shown to prevent tumorigenesis in an animal model.

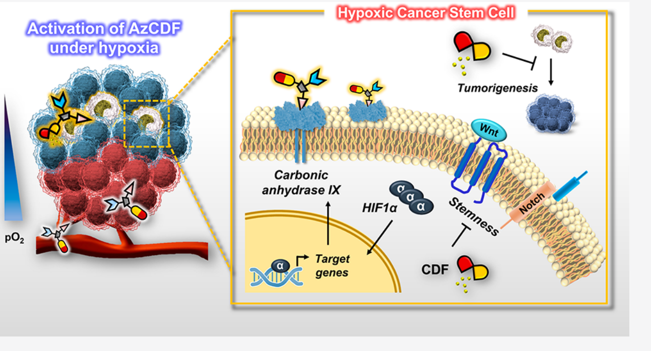

■ INTRODUCTION

Cancer stem cells (CSCs), also known as tumor-initiating cells (TICs), are a subset of cancer cells characterized by a capacity for initiating tumor growth, metastasis, self-renewal, and differentiation. These cells have been found to contribute to tumor regrowth, metastasis, and recurrence.[1,2] Despite major therapeutic advances in recent years, drug resistance and cancer recurrence limit the success of standard therapeutic interventions. In heterogeneous breast cancers, a subset of breast cancer stem cells (BCSC) are strongly correlated to tumorigenesis, chemoresistance, and poor patient prognosis, a result ascribed to their recognized ability to undergo self-renewal. There is a growing body of evidence that CSCs are implicated in tumor relapse due to their innate chemoresistance. As such, they represent a clinical obstacle to effective tumor therapy.[3,4] Under normal conditions, CSCs cells are dormant and are thus highly resistant to chemotherapeutics designed to target rapid cell proliferation.[5,6] Certain stimuli have the potential to activate these cells, resulting in rapid differentiation and ultimately tumorigenesis. Thus, a major goal in CSC research is to develop new strategies that could be used to identify and eradicate effectively chemoresistant CSCs.[7] Not surprisingly, therefore both diagnostic tools and therapeutic agents that target CSCs are highly sought after;[8] however, to date only limited progress has been made.[9−15] Here report what we believe is the first small molecule construct capable of targeting CSCs, decreasing their migration, and preventing tumorigenesis, as inferred from both in vitro and in vivo mouse model studies. Modification to the system provides access to a congener that allows for the fluorescence-based detection of CSCs in vitro. Both systems rely on targeting hypoxic tumor regions.

Hypoxia is a particular feature of various solid tumors that results inter alia from tumors outgrowing their blood supply as well as a lack of fully functional blood vessels within tumors.[16−18] CSCs have been found to exist mainly within these oxygen-deprived tumor regions, and maintaining a

Received: April 13, 2021

hypoxic microenvironment is considered crucial to the self-renewal of CSCs as well as the expression of stem cell factors such as Oct4, c-Myc, and Nanog.[3,18] Furthermore, potential roles for Notch and Wnt signaling in CSC proliferation, metastasis, and stemness have been suggested in breast and gastric cancer.[19−21] Thus, targeting hypoxic microenvironments could provide an approach to eliminating CSC populations.

Small-molecule drug delivery systems (DDSs) provide an attractive approach to targeting tumor microenvironments and to controlling the conditional release of cytotoxic agents and/or imaging agents.[22] Given that CSCs preferentially survive in hypoxic microenvironments, we designed a tailor-made hypoxia-activated small-molecule prodrug system. It has been noted that high levels of reductive enzymes in hypoxic tissues can be exploited to affect the conditional activation of imaging probes and prodrugs.[23] This is an approach we have adopted here to effect the efficient directed delivery of a putative anti-CSC drug, 3,4-difluorobenzylidene curcumin (CDF). Our release system relies on dimethylnitrothiophene, which has a lower reduction potential compared to the more widely used nitrobenzene redox-active hypoxic trigger. The dimethyl group is also thought to stabilize the transition state of the cleavage reaction which occurs following initial reduction of the targeting group, thereby allowing for favorable reaction kinetics.[24−26] This, as detailed below, has allowed us to create a new multimodal drug conjugate, **AzCDF**, which targets CSCs through carbonic anhydrase IX (CAIX) inhibition (Figure 1a). A closely related analogue, **AzNap**, designed to release a fluorophore in a similar fashion, was also prepared to allow for fluorescence-based CSC imaging.[27]

CAIX is a transmembrane protein that is induced under hypoxic conditions. As such, it has been used as a biomarker for hypoxia.[28] The enzyme regulates the extracellular pH and contributes to the often observed decreased extracellular pH in solid tumors in a process known as tumor acidification. Hypoxia-induced upregulation of CAIX has been associated with poor prognoses, while the inhibition of CAIX has been demonstrated to lead to significant growth suppression and decreased rates of metastasis in vivo.[29−31] Importantly, these effects appear to correlate, at least in part, with a reduction in CSC levels. For instance, acetazolamide (Az), a well-known inhibitor of CAIX, has been noted to reduce CSC levels.[28] Hence, we decided to use Az as a targeting agent and secondary therapeutic in our CDF-containing multimodal conjugate **AzCDF**.

CDF is a synthetic analogue of curcumin, available from this natural product through a simple one-step Knoevenagel condensation reaction. Several literature reports have suggested that curcumin could be a potential therapeutic for the suppression of CSCs; however, its poor bioavailability and the need for high concentrations have raised concerns.[32−34] More broadly, the therapeutic use of curcumin as a therapeutic modality remains highly controversial due, for example, to its reactivity and potential for covalent protein labeling. This has led curcumin to be described as a PAIN (pan-assay interference compound).[35] On the other hand, CDF appears devoid of this undesired reactivity and exhibits not only an increased metabolic stability but also a greatly enhanced cytotoxicity toward chemotherapy-resistant CSCs.[36,37] Moreover, CDF modulates multiple molecular targets, such as stemness-related marker genes and microRNAs, providing a strong mechanistic rationale for effective CSC elimination.[38]

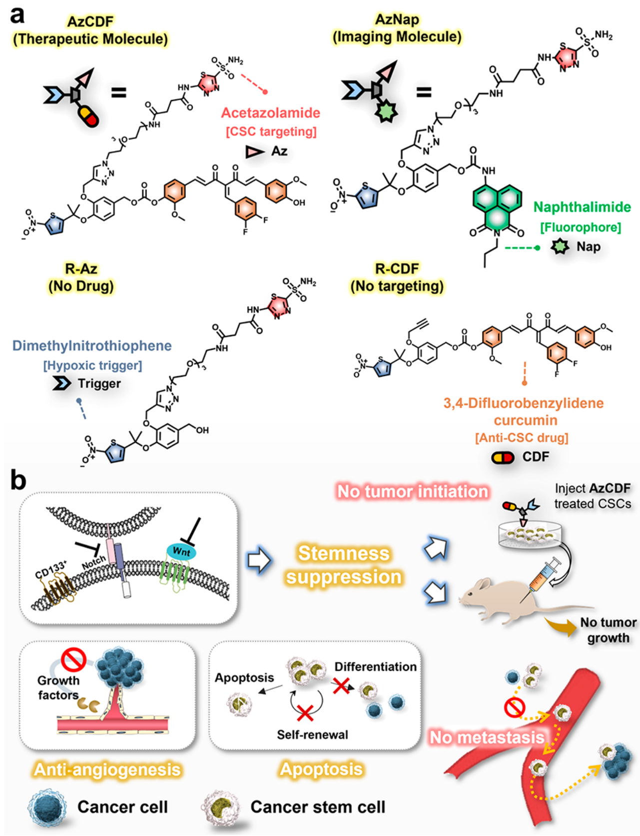

Figure 1. Schematic overview of the mode of action proposed for the multimodal conjugate of this study (**AzCDF**). (a) Chemical structure and components of **AzCDF**, **AzNap R-Az, and R-CDF**. (b) Proposed mechanism of CSC deactivation by **AzCDF**.

In light of the above considerations, we designed **AzCDF** as a DDS platform to deliver CDF selectively to CAIX-expressing hypoxic CSCs. As discussed further below, we observed the selective eradication of CSCs in hypoxic breast cancer tumors, both in vitro and in vivo (Figure 1b). Importantly, we also observed decreased CSC migration in vitro as well as decreased tumor growth and lowered tumorigenesis rates in mouse models.

■ RESULTS AND DISCUSSION

Design, Synthesis, and Characterization of AzNap and AzCDF. The conjugates **AzCDF** and **AzNap** were designed to target CSCs and allow delivery of an active payload, CDF, or a fluorophore, naphthylimide, under hypoxic conditions. These constructs were prepared as shown in Scheme S1. Also prepared were two reference systems lacking (i) the proposed CSC targeting unit (**R-CDF**) or (ii) the putative drug moiety (**R-Az**). The synthesis of these four agents is detailed fully in the Supporting Information. Briefly, compound **6** was prepared via a Mitsunobu reaction performed in the presence of 1,1′-(azodicarbonyl)dipiperidine (ADDP) and tributylphosphine (PBu_3) in accord with a protocol used to activate less reactive tertiary alcohols.[26] A subsequent reduction of the aldehyde resulted in compound **7**, which served as a common intermediate for all four final compounds.

Starting from **7**, activation of the alcohol followed by reaction with CDF resulted in **R-CDF**, while a similar synthetic pathway using phosgene (*caution: highly toxic*) was used to generate the naphthylimide-containing precursor **4**, again starting from 7. A final CuACC click reaction between **4** and the azide-labeled Az derivative **9** yielded **AzNap**, while the same reaction of **4** with **7** resulted in **R-Az**. Activation of the alcohol present in **R-Az** with *p*-nitrophenyl chloroformate, followed by a substitution reaction with CDF, yielded **AzCDF**. Full characterization data (^{1}H and ^{13}C NMR spectroscopy and ESI-MS) for all new compounds can be found in the Supporting Information (Figures S1−S31). UV−vis spectra of **AzNap** and **AzCDF** were also recorded, and a characteristic absorbance peak was observed at 370 and 330 nm, respectively (Figure S32).

In Vitro Reductive Activation of AzNap and AzCDF. A depiction of the proposed release of the active fluorophore and proposed therapeutic payload, CDF, from **AzNap** and **AzCDF**, respectively, under model hypoxic conditions is provided in Figure 2a,b. Here, reduction of the dimethylnitrothiophene

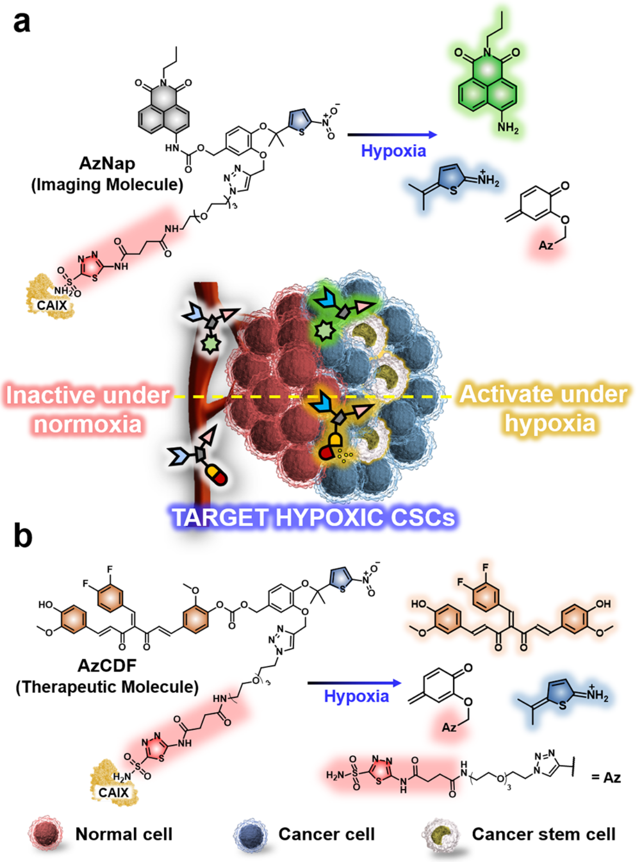

Figure 2. Chemical structures of (a) **AzNap** and (b) **AzCDF** and the activation mechanism proposed to be operative under hypoxic conditions.

group and subsequent release of the fluorophore or CDF were assessed by using *E. coli* nitroreductase (NTR) in the presence of NADH as a model reductant.[23,39] As can be seen in Figure 3a,b, a concentration- and time-dependent fluorescence emission feature at 540 nm is seen in the case of **AzNap** with saturation being reached within 30 min. This finding is consistent with the proposed release of the fluorescent dye (Figure S33). **CDF** has a weak but significant absorbance with a maximum intensity around 450 nm. A similar release profile was anticipated for **AzCDF**. In fact, when **AzCDF** was subjected to the model reductive conditions used for **AzNap**, an absorbance feature specific to CDF was seen (Figure 3c).

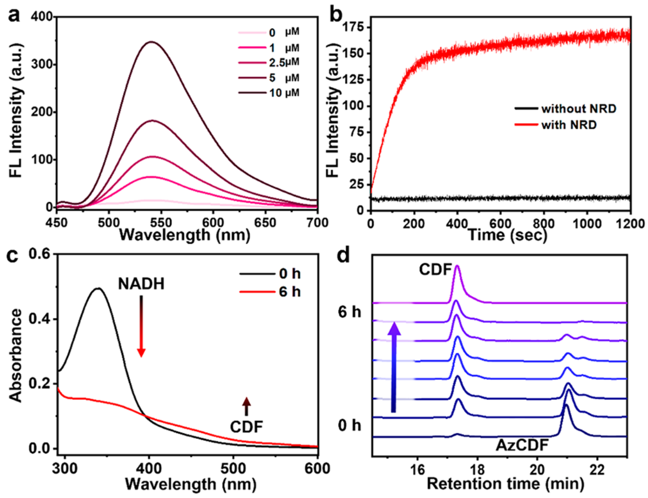

Figure 3. (a) Concentration-dependent fluorescence of **AzNap** (0−10.0 μM) recorded after incubating with nitroreductase (10 μg/mL) and NADH (50 μM) for 30 min in PBS (pH 7.4) at 37 °C (λ_{ex} = 432 nm). (b) Time-dependent fluorescence of 5 μM **AzNap** with and without nitroreductase (λ_{em} = 550 nm). (c) UV/vis spectrum of **AzCDF** (5 μM) before and after the addition of 10 μg/mL nitroreductase and NADH (50 μM). (d) HPLC analysis (absorbance at 365 nm) of 5 μM **AzCDF** incubated with 10 μg/mL nitroreductase and 50 μM NADH at 37 °C for the indicated times. Also shown are the chromatograms of **AzCDF** and CDF.

Moreover, an HPLC assay revealed the absence of **AzCDF** and the full release of CDF within 6 h (Figure 3d). On this basis, we considered it likely that both **AzNap** and **AzCDF** would target CSCs in hypoxic tumor environments.

Validation of AzNap and AzCDF Activation in Hypoxic CSCs. As a predicate to further analyses, CD133^{+} cells, a common biomarker of cancer stemness,[18,40,41] were sorted by using magnetic-activated cell sorting (MACS)[42] (Figure 4a and Figure S34). While a 2−4% population of CD133^{+} cells in multiple breast cancer cell lines was reported in a prior study,[41] in our hands we found that 17% of MDA-MB-231 cells carried the CD133 antigen. We confirmed the presence of the antigen with Western blotting, reflecting a strong enrichment of CD133 following MACS sorting, with the expression of CD133 being maintained through the second subculture (Figure 4b).

The potential delivery of the drug conjugate used in this study (**AzCDF**) was assessed by using the fluorescent surrogate **AzNap**. As can be seen in Figure 4c and Figure S35, the bright green fluorescence originating from the naphthalimide released from **AzNap** could clearly be observed for cancer cells maintained under mild hypoxic conditions (3% O_2). This relatively high sensitivity of the dimethylnitrothiophene trigger to hypoxia demonstrates the benefit of this triggering unit as compared to nitrobenzene-based triggers, a linker moiety that frequently requires severe hypoxia (0.5−1% O_2) to undergo reductive activation.[43,44] No fluorescence ascribable to cleaved **AzNap** was observed under normoxia or when noncancerous BJ cells lacking CAIX expression were tested. On the other hand, the fluorescent intensity of **AzNap**-treated CD133^{+} cells was ∼24% brighter compared to unsorted MDA-MB-231 cells (Figure S36). This observation is ascribed to CAIX-promoted uptake of **AzNap** and reflects the overexpression of CAIX in hypoxic CD133^{+} MDA-MB-231 cells (Figure S37).[45] To provide support for this proposed

https://doi.org/10.1021/jacs.1c03875
J. Am. Chem. Soc. XXXX, XXX, XXX−XXX

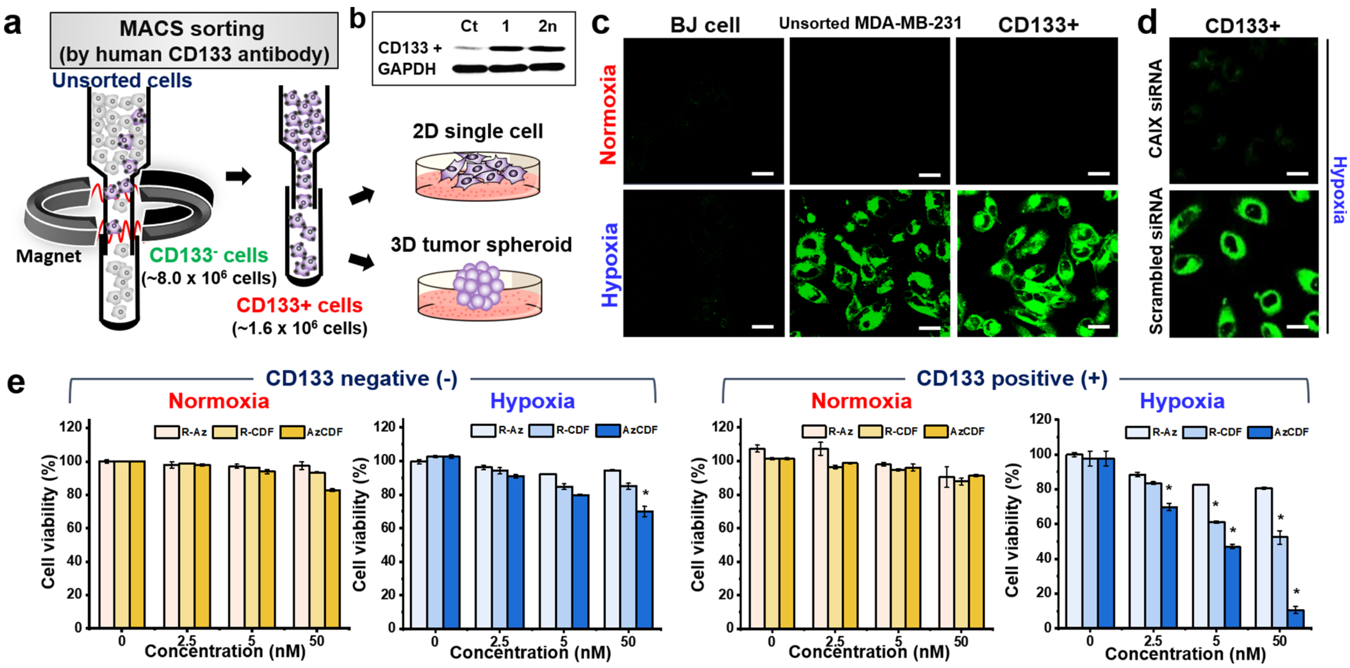

Figure 4. In vitro effects of **AzNap** and **AzCDF**. (a) Graphical representation of magnetic-activated cell sorting (MACS) of MDA-MB-231 cells based on the expression of the CSC marker CD133 as well as their 2D and 3D cell cultures. (b) Western blot analysis of the expression of unsorted MDA-MB-231 as well as the MACS-sorted $CD133^+$ population after the first and second subculturing. (c) In vitro fluorescence of different cells and cell populations incubated with **AzNap** under normoxia and 3% O_2. Magnification: 200×; scale bar: 50 μm. (d) CAIX knock-down $CD133^+$ MDA-MB-231 cells, and scrambled siRNA control cells, were treated with **AzNap** under 3% O_2. (e) Cytotoxicity (MTT assay) of $CD133^-$ and $CD133^+$ cells under normoxia and 3% O_2, incubated for 24 h with **AzCDF**, or the reference systems **R-Az** and **R-CDF**. *p < 0.05, relative to the corresponding untreated groups.

uptake mechanism, we used a CAIX siRNA-mediated gene knockdown cell model. A bright fluorescence resulting from **AzNap** activation could only be observed for $CD133^+$ MDA-MB-231 cells treated with a scrambled siRNA control, when maintained under 3% O_2. We take this finding as evidence that CAIX is involved in the cellular uptake of **AzNap** (Figure 4d and Figure S38).

To support the contention that hypoxia is a prerequisite for payload release, a cover glass was positioned partially over a slide with MDA-MB-231 cells. Appreciable fluorescence was seen only for the oxygen-starved cells underneath the cover glass (Figure S39). Taken together, these results are consistent with the design expectation that **AzNap** uptake occurs selectively in CAIX-expressing cells and that activation of the drug delivery platform is limited to cells maintained in hypoxic environments.

The intracellular localization of naphthalimide fluorescence could not be pinpointed to a single organelle type; rather, fluorescence was seen in the mitochondria, endoplasmic reticulum, and lysosomes (Figure S40). This is taken as evidence that, upon the recognition of the Az targeting group by the transmembrane protein CAIX, **AzNap** is taken up by the cell and that it or its released fluorophore payload is distributed throughout the cell. Given the structural similarity involved, **AzCDF** is believed to exhibit similar uptake and subcellular biodistribution behavior.

The therapeutic potential of **AzCDF** was assessed by using cell viability assays; these revealed an increased cellular toxicity in several cancerous cell lines, including MDA-MB-231, HepG2, and MCF7 cells, albeit only under hypoxic conditions (Figure S41). As the concentration and incubation time increased, the cellular toxicity became more pronounced under hypoxia. This finding is ascribed to the selective activation of **AzCDF** under conditions of hypoxia and to the fact that CAIX is a hypoxia-induced upregulated gene.[46] Support for this conclusion came from Western blot analyses of the CAIX expression levels under normoxic and hypoxic environments in these three cell lines (Figure S42). The cytotoxicity of **AzCDF** and reference compounds not bearing a targeting or drug, **R-CDF** and **R-Az**, was assessed under normoxic and hypoxic conditions for both $CD133^+$ and $CD133^-$ MDA-MB-231 cells, demonstrating strikingly different behavior (Figure 4e and Figure S43). As would be anticipated based on our design strategy, the cell viability remained largely unaffected by the presence of **AzCDF**, **R-CDF**, or **R-Az** under normoxic conditions. This was taken as further evidence of the stability of the dimethylnitrothiophene trigger (and corresponding lack of drug release) except under conditions associated with reductive metabolism.

For both the $CD133^+$ and $CD133^-$ MDA-MB-231 cell populations, a dose-responsive dependence on the **AzCDF** cytotoxicity was observed with higher toxicity being seen in the $CD133^+$ cell population. This result reflects, presumably, a greater degree of **AzCDF** uptake in these CAIX-expressing cells. It thus mirrors the increased fluorescence intensity of **AzNap** seen in these cells as well as the Az-induced CSC depletion reported previously.[47−49] Notably, while **AzCDF** demonstrated the most significant cytotoxicity under hypoxic conditions, the toxicity of **R-CDF** was low, but not negligible, under these conditions. This finding is attributed to both the release of a quinone methide (and an analogous reactive thiophene derivative; see Figure 2) as well as the inherent Az activity. This leads us to suggest that the action of **AzCDF**

https://doi.org/10.1021/jacs.1c03875
J. Am. Chem. Soc. XXXX, XXX, XXX−XXX

depends not only on CDF release and CAIX inhibition but also on quinone methide generation (vide infra).

Studies of Tumorigenesis Using 3D Tumor Spheroids. To investigate further the presumed hypoxic activation of **AzNap** and **AzCDF**, three-dimensional tumor spheroids were used. Tumor spheroids are considered to be good model systems in that they mimic several key features of solid tumors. Most notably, both the spheroids and solid tumors possess a hypoxic inner core reflecting oxygen transport to the core cells that is diffusion limited in both cases.[50]

In this study, we used MDA-MB-231 tumor spheroids derived from unsorted cells as well as $CD133^-$ and $CD133^+$ cell populations. As can be seen in Figure 5a, tumor spheroids coincubated with **AzNap** under normoxic conditions were characterized by a higher level of fluorescent $CD133^+$ cells relative to unsorted MDA-MB231-cells or $CD133^-$ cells. This fluorescence is attributed to the activation of **AzNap** in the hypoxic core of the spheroid. Evidence to support the presence of a hypoxic core in these spheroids was provided by the expression of HIF1α, a key marker of cellular hypoxia, in a time-dependent manner (Figure S44). This finding provides support for the hypothesis underlying this study, namely, that the CAIX homing and associated hypoxia-dependent payload release benefits from CSC selectivity that is operative not only in primary cell cultures but also in tissue-mimicking tumor spheroids.

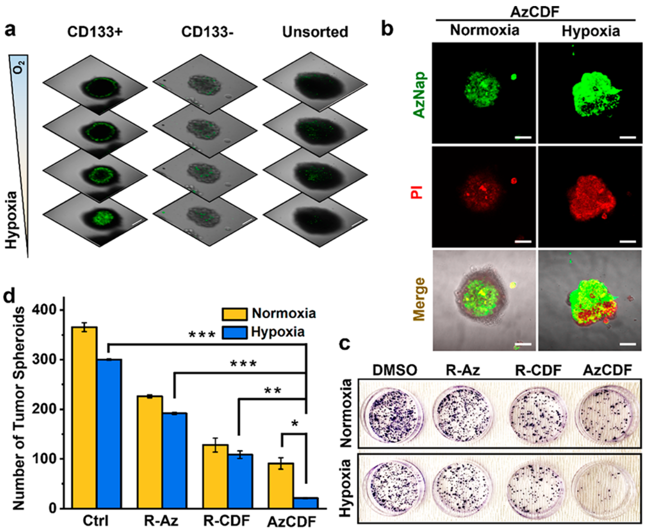

Figure 5. Fluorescent images and effect of **AzNap** and **AzCDF** in tumor spheroids. (a) Unsorted MDA-MB-231 cells as well as sorted MDA-MB-231 $CD133^-$ and $CD133^+$ cells were incubated in ultralow attachment dishes to promote tumor spheroid formation and grown under normoxic conditions for 2 days. **AzNap** (5.0 nM) was added, and the spheroids were further maintained under normoxic conditions. A *z*-stacked fluorescence analysis was performed on the fifth day. The bright fluorescence of **AzNap**-treated spheroids under normoxia is taken as evidence of the natural hypoxia that pertains in these spheroids. Scale bar: 100 μm. (b) Double **AzNap** and PI staining of **AzCDF**-treated $CD133^+$ MDA-MB-231 tumor spheroids. Spheroids were treated with **AzNap** and **AzCDF** (5.0 nM each) on the second day, PI was added on the third day, and cryosection analyses were performed on the fifth day. Scale bar: 100 μm. (c) $CD133^+$ MDA-MB-231 cells were seeded in ultralow attached dishes, grown under normoxic conditions for 2 days, followed by 3 days under either normoxic or 3% hypoxic conditions with control, **R-Az**, **R-CDF**, or **AzCDF** (5.0 nM). The tumor spheroids were transferred into 35 mm cell culture dishes. The next day, the attached spheroids were stained with 20% crystal violet solution. (d) Quantitative analysis of the number of tumor spheroids formed in panel c. $^{*}p < 0.05$, $^{**}p < 0.01$, and $^{***}p < 0.005$.

Based on the above imaging studies, tumor spheroids were treated with **AzCDF**. The resulting tumor spheroids were cryosectioned and stained with propidium iodide (PI) and Calcein-AM (Figures S45). Red fluorescence from PI, indicating dead cells, was seen in the spheroids grown under hypoxic conditions, while the green fluorescence originating from calcein-AM, indicating live cells, was reduced. The DMSO-treated controls, maintained under either normoxia or 3% O_2, showed no fluorescence from PI. Consequently, **AzCDF** and **AzNap** were used to cotreat spheroids with PI staining to test their simultaneous function (Figure 5b). Spheroids grown under normoxia showed a distinct pattern corresponding to the spheroid core. In contrast, the spheres grown under 3% O_2 showed both PI and naphthalimide fluorescence signals throughout the entire area of the sphere.

To assess the self-renewal capacity of these $CD133^+$ MDA-MB-231 tumor-initiating cells, tumor spheroids were treated with 5.0 nM of either **R-Az**, **R-CDF**, or **AzCDF** on the second day of spheroid formation and were randomly selected for further incubation under normoxic or hypoxic conditions (3% O_2). On the fifth day, analysis revealed that fewer spheroids remained under hypoxic conditions, with the largest reduction in spheroid numbers being seen for the **AzCDF**-treated hypoxia-incubated cells (Figure 5c,d). Not only is the number of surviving spheroids particularly low in the **AzCDF**-treated groups, but the size reduction is also significant (Figure S46). **AzCDF**-treated normoxic and hypoxic spheroid structures are smaller in size and often demonstrate a damaged morphology, while DMSO-treated control spheroids are larger and do not exhibit signs of damage (Figure S47). On this basis, we conclude that the released CDF effectively kills the CSCs, resulting in a downregulating of the tumor initiating properties. The spheroids grown under normoxic conditions also demonstrated some reduction in viability. This finding is rationalized in terms the cells grown under normoxic conditions being less affected at the outset; however, over time a hypoxic core is produced that triggers CDF release.

Mechanistic Studies. The determinants of CDF-induced growth inhibition and apoptosis of CSCs are multifactorial and are reported to be mediated through the downregulation of EGFR, IGF-1R, NF-κB, c-Myc, β-catenin, COX-2, and Bcl-xL signaling, membrane transporter ABCG2, and miRNA-21, which are considered crucial for the maintenance of CSC stemness.[51] As a predicate to our own studies, the expression of the stemness factors Oct4 (required for expression of CSCs in a breast luminal progenitor), Nanog homeobox (Nanog), SRY-box transcription factor 2 (Sox2), Myc proto-oncogene protein (*c*-Myc), Notch homologue 1 (Notch1), Wnt Family Member 1 (Wnt1), and β-catenin was determined by using quantitative polymerase chain reaction (qPCR) analyses. Gene expression levels were compared between unsorted MDA-MB-231 and $CD133^+$ cell populations. Overexpression of the monitored stemness factor genes was found for the $CD133^+$ cells (cf. Figure S48), a finding in accord with the canonical thinking that this cell population exhibits strong stemness characteristics.

$CD133^+$ cells were incubated with 5.0 nM of the reference compounds **R-Az** and **R-CDF** as well as **AzCDF**. Compared to the untreated control group, **R-Az** and **R-CDF** gave rise to

https://doi.org/10.1021/jacs.1c03875
J. Am. Chem. Soc. XXXX, XXX, XXX−XXX

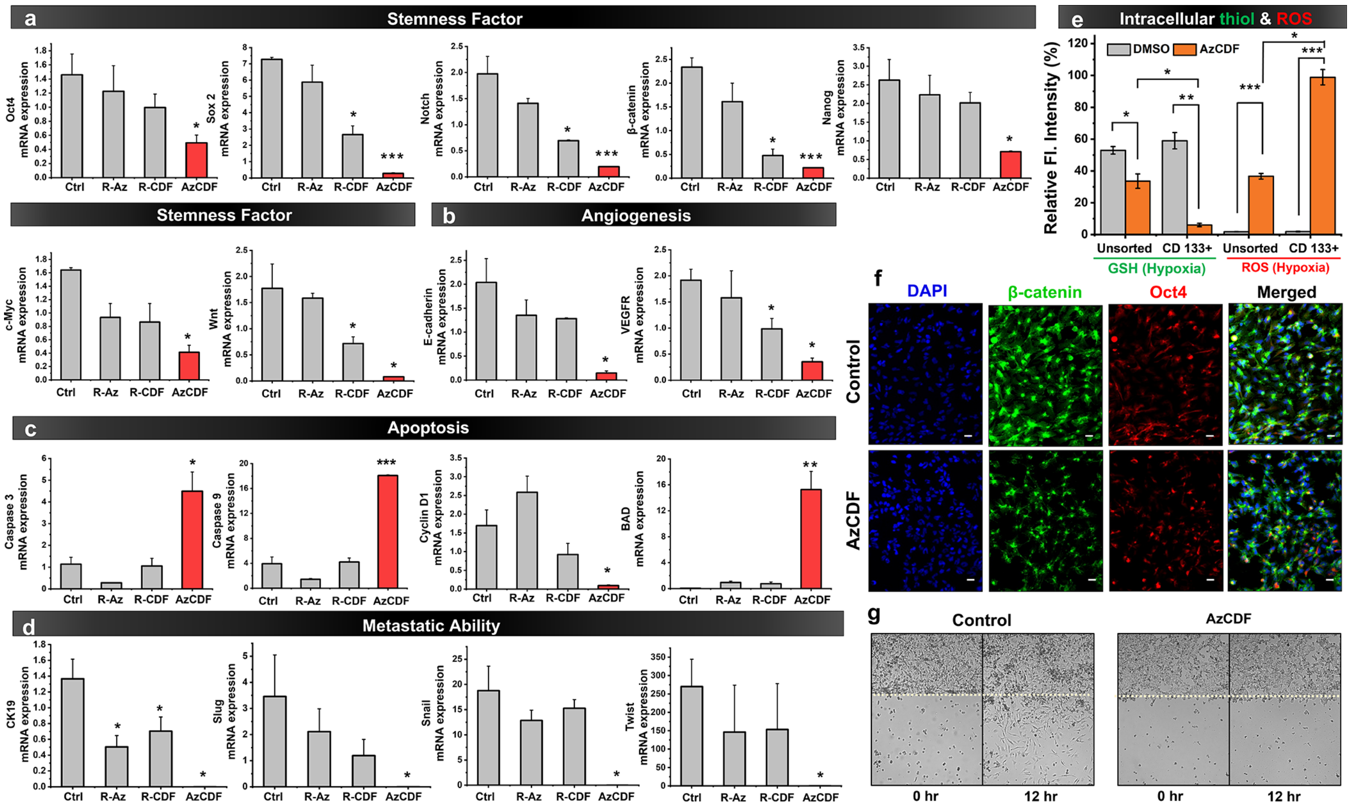

Figure 6. Investigation of the mechanisms by which **AzCDF** suppresses stemness in adherent CD133$^+$ CSCs. Quantitative PCR analyses of relative mRNA levels after 24 h incubation with 5.0 nM **AzCDF**, **R-Az**, or **R-CDF** and control consisting of DMSO in CD133$^+$ MDA-MB 231 cells. (a) Stemness markers (Oct4, Sox2, Nanog, c-Myc, Notch1, Wnt1, and β-catenin), (b) angiogenetic markers (E-cadherin and VEGF), (c) apoptotic markers (Cyclin D1, Caspase 3, Caspase 9, and Bad), and (d) metastasis related markers (CK19, Slug, Snail, and Twist). Data represent the mean ± SE; *$p < 0.05$, **$p < 0.01$, ***$p < 0.001$ relative to the control group. All values presented are normalized to the relative gene expression levels of the target gene by using GAPDH as a reference. (e) Quantitative analysis of intracellular GSH depletion and ROS generation under 3% hypoxia. Intracellular GSH content: green thiol tracker. ROS: MitoSox red. Unsorted and CD133$^+$ MDA-MB$^-$231 cells were incubated under the presence of **AzCDF** (5.0 nM) or DMSO as a control for 24 h. *$p < 0.05$, **$p < 0.01$, and ***$p < 0.005$ relative to the corresponding DMSO-treated groups. (f) Immunohistochemical analyses (CD133$^+$ cells treated with 5.0 nM **AzCDF** under normoxic or 3% hypoxic conditions) using fluorescent antibodies for Oct4 (red) and β-catenin (green) as well as the nucleus marker DAPI (blue) Magnification: 200×; scale bar: 50 μm. (g) Migration assay of CD133$^+$ cells before and after treating with DMSO or **AzCDF**.

somewhat reduced Nanog and Wnt gene expression. In contrast, statistically significant gene suppression of the Oct4, Nanog, Sox2, c-Myc, Notch1, Wnt1, and β-catenin was seen in the **AzCDF**-treated group (Figure 6a). These stemness-related genes are thought to play critical roles in maintaining the proliferation and metastasis of CSCs.[52,53] Among these suppressed genes, Sox2 has recently been reported to promote anticancer drug resistance and CSC proliferation via Sox2-dependent activation of Wnt signaling.[54,55] Protein levels of Oct4 and β-catenin were also investigated in the **AzCDF**-treated normoxia and hypoxia CD133$^+$ CSCs by immunohistochemistry (Figure 6f). The results proved concordant with those of the qPCR analyses, with strongly diminished Oct4 and β-catenin protein concentrations being found after treatment with nanomolar concentrations of **AzCDF** (Figure 6a).

E-cadherin and VEGFR are typical migration and angiogenesis related markers, respectively. These genes were also suppressed by **AzCDF** treatment in CD133$^+$ MDA-MB-231 cells (Figure 6b). These findings are thus consistent with a previous study that curcumin inhibits the migration of breast CSC via suppressed E-cadherin/β-catenin signaling.[56] Additionally, the apoptotic genes (Caspase 3, Caspase 9, and BAD) were significantly increased, whereas Cyclin D1 was decreased (Figure 6c).

In addition to liberating a putative anticancer agent per se, the release of CDF from **AzCDF** generates 2 equiv of quinone methide (Figure S50a). Quinone methides are known to produce reactive oxygen species (ROS) due to intracellular glutathione (GSH) depletion.[57−60] This latter effect could account for the hypoxic toxicity of **R-Az** and **R-CDF** noted above. Consistent with this hypothesis, the fluorescent intensities of a thiol tracker were significantly reduced in both **AzCDF**-treated unsorted cells and virtually absent in the CD133$^+$ cells; this is as would be expected for a reduction in intracellular GSH levels (Figure 6e). As GSH is involved in ROS quenching, the reduction of GSH concentrations could account for the high intracellular ROS concentrations seen upon treatment with **AzCDF** under hypoxia. DMSO-treated hypoxic cells showed negligible differences with those incubated under normoxia. This further supports the contention that GSH depletion and ROS increases result from the hypoxia-induced activation of **AzCDF** (Figure S50b,c). The ROS and thiol levels of CD133$^+$ spheroids grown under normoxic or hypoxic conditions after the second day, treated with either DMSO or **AzCDF**, were found to differ significantly (Figure S50d). These findings thus lend credence to the hypothesis that both hypoxia and **AzCDF** are required

https://doi.org/10.1021/jacs.1c03875
J. Am. Chem. Soc. XXXX, XXX, XXX−XXX

for the generation of quinone methides and the triggering of the observed changes in cellular ROS/thiol levels.

On the basis of the above studies, we propose that the CSC suppressive effect of **AzCDF** is a result of both CDF release and perturbations of the intracellular redox balance. The mortality of breast cancer is strongly associated with the emergence of distant metastases. In the process of metastasis, CSCs undergo a genetic progression, called epithelial to mesenchymal transition (EMT), that is thought to promote migration into the surrounding tissues. CK19, Snail, Slug, and Twist are known metastatic markers, and their increased expression in breast cancer patients is correlated with a poor prognosis.[61] Previous studies have led to a consensus view that CK19 and Twist are expressed early on in the course of disease progression and contribute to metastasis by advancing EMT.[62,63] Snail and Slug, zinc-finger domain transcription factors, play a key role in EMT, triggering metastatic characteristics of breast cancer cells.[64] As expected, metastatic marker genes are highly expressed in CD133$^+$ MDA-MB-231 cells as compared to unsorted cells (Figure S50). However, **AzCDF** was able to reverse this in CD133$^+$ cells, with virtually no migration (Figure 6g, Video S1, and Video S2) and significantly decreased levels of EMT markers being seen (Figure 6d).

In Vivo Therapeutic Effect of AzCDF and Selective Fluorescence Imaging of AzNap. To test whether the tumor and CSC homing of the present drug delivery platform is effective in vivo, we performed studies using MDA-MB-231 cell xenograft-bearing mice. As shown in Figure 7a and Figure S51, after a single tail-vein injection of **AzNap**, fluorescence emanating from the xenografts could be observed readily and was still significant 144 h postinjection. Ex vivo imaging of excised tissues confirmed a strong fluorescence corresponding to the tumors but virtually no fluorescence from any of the vital organs (Figure 7b). MDA-MB-231 cell xenograft-bearing mice treated with a control solution, **R-Az**, **R-CDF**, or **AzCDF**, via tail vein injection (once a week for 3 weeks) revealed tumor growth rates that were most strongly reduced in the case of the **AzCDF**-treated mice (Figure 7c,d). The relatively smaller growth reductions seen for the **R-Az** or **R-CDF** groups is consistent with our design expectations, namely, that both a potent drug (CDF) and Az-based CSC targeting are needed to produce a strong antitumor effect. The compound-dependent in vivo tumor growth reduction was mirrored in the size differences seen for the excised tumors (Figure 7e). Importantly, the agents of this study were generally well tolerated, as reflected in the final body weights (Figure S52) and the lack of major pathological signs when slides from the vital organs were subject to H&E staining (Figure S53).

In Vivo Tumorigenesis Study. To assess the ability of **AzCDF** to prevent tumorigenesis in vivo, CD133$^+$ MDA-MB-231 cells were first sorted by MACS per the protocol of Figure 4a as discussed above. These cells were then incubated with either DMSO or **AzCDF** under hypoxic conditions for 6 h. The number of live cells was determined by using trypan blue, and the same number of lives cells from both incubation protocols was injected into nude mice to determine the extent of tumor initiation (Figure 7f). The use of hypoxic conditions prior to injection into the mice was deemed necessary since, particularly in the case of **AzCDF**, it was necessary to keep the cells alive while suppressing their stemness. After 6 weeks, a remarkable and statistically significant difference in tumorigenesis was observed without effecting the body weight of the mice (Figure 7g,h and Figure S54) in the case of the animals injected with the **AzCDF**-treated cells. In contrast, the mice injected with the same number of DMSO-treated cells showed rapid tumor growth. Taken in concert, the results of this tumorigenesis study are in line with the mechanistic analysis above wherein **AzCDF** served to suppress stemness related genes and proteins. We thus conclude that **AzCDF** embodies a

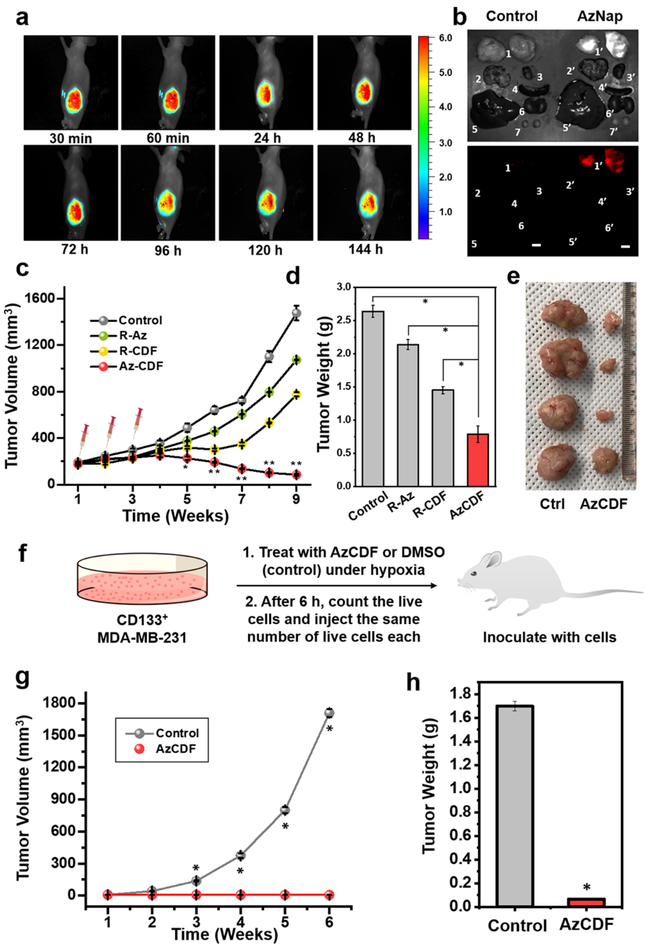

Figure 7. In vivo xenograft tumor imaging and treatment using **AzNap** and **AzCDF**, respectively. (a) In vivo fluorescent images of xenograft BALB/C nude mice recorded at various time points after intravenous injection of **AzNap** (50.0 nM in 100 μL of PBS) into the tail vein. Injections were once a week for 3 weeks (total of three injections). (b) Ex vivo fluorescence of various tissues following **AzNap** administration alongside a PBS reference (1 and 1′: tumor; 2 and 2′: lung; 3 and 3′: heart; 4 and 4′: spleen; 5 and 5′: liver; 6 and 6′: kidney; 7 and 7′: testes. (c) Tumor volume of the mice in different treatment groups ($n = 8$ mice, total 16 tumors). Tail-vein injection of **R-Az**, **R-CDF**, or **AzCDF** (50.0 nM in 100 μL of PBS) was performed once per week for 3 weeks, for a total of three injections. $*p < 0.05$ and $**p < 0.005$; **Az-CDF** with control and **R-Az** and **R-CDF**, respectively. (d) Average tumor weight of each of the treatment groups at the end of the experiment. $*p < 0.005$. (e) Representative images of excised tumors. (f) Test of the in vivo tumorigenesis potential of CD133$^+$ MDA-MB-231 cells, treated with either **AzCDF** or DMSO. (g) CD133$^+$ MDA-MB-231 cells were treated with either DMSO as control or 5.0 nM **AzCDF** for 24 h, and then the cells were inoculated into mice to examine tumorigenesis. As noted in the main text, the same number of cells was used in both cases. The plot shows tumor volume vs time. Tumor volume and (h) weight of excised tumors from the study in 6 weeks after inoculation ($n = 6$ mice, total 12 tumors). $*p < 0.005$.

https://doi.org/10.1021/jacs.1c03875
J. Am. Chem. Soc. XXXX, XXX, XXX−XXX

potentially powerful strategy that can be used to overcome tumorigenesis attributed to CSCs.

■ CONCLUSIONS

In summary, we have developed the paired molecular platforms **AzNap** and **AzCDF** for imaging and therapeutic intervention, respectively. Both probes were designed to target CSCs. The requisite CSC targeting was achieved by using a CAIX-targeting ligand. In the case of **AzCDF**, conditional release of an active subunit, CDF, occurs under hypoxic conditions. This agent was found to give rise to a statistically significant reduction in cell viability especially in the $CD133^+$ CSC population of MDA-MB-231 cells. The potency of the released drug, CDF, is thought to be further amplified by a disruption of redox homeostasis, an effect seen most profoundly in the sorted $CD133^+$ cells. In vitro under mild hypoxia (3% O_2), **AzCDF** was characterized by a single digit nanomolar IC_{50} value, while virtually no toxicity was observed under normoxic conditions. The cell-based results translated well to an in vivo setting, as reflected in the clear attenuation of MDA-MB-231 cell xenograft tumors in mouse models upon **AzCDF** administration. Effective inhibition of tumorigenesis in vivo was also seen. Overall, **AzCDF** represents a potential step forward in the selective eradication of CSCs and one that may in due course allow tumor recurrence to be overcome. **AzNap** provides a complement to **AzCDF** that could prove useful for the early diagnosis of highly aggressive cancers. The present study serves to underscore the role that multimodal agents may have to play in overcoming the poor clinical outcomes ascribed to breast cancer stem cells (BCSCs).

■ ASSOCIATED CONTENT

Supporting Information

The Supporting Information is available free of charge at https://pubs.acs.org/doi/10.1021/jacs.1c03875.

Detailed experimental conditions and methods, synthesis, structural characterization, subcellular localization, functional characterization of biological evaluations (PDF)

Video S1 (MP4)

Video S2 (MP4)

■ AUTHOR INFORMATION

Corresponding Authors

Jiyou Han − *Department of Biological Sciences, Hyupsung University, Hwasung-si 18330, Korea*; Email: hanjiyou12@hanmail.net

Jong Seung Kim − *Department of Chemistry, Korea University, Seoul 02841, Korea*; orcid.org/0000-0003-3477-1172; Email: jongskim@korea.ac.kr

Jonathan L. Sessler − *Department of Chemistry, The University of Texas at Austin, Austin, Texas 78712, United States*; orcid.org/0000-0002-9576-1325; Email: sessler@cm.utexas.edu

Authors

Ji Hyeon Kim − *Department of Chemistry, Korea University, Seoul 02841, Korea*

Peter Verwilst − *Department of Chemistry, Korea University, Seoul 02841, Korea*; orcid.org/0000-0002-4673-2050

Miae Won − *Department of Chemistry, Korea University, Seoul 02841, Korea*; orcid.org/0000-0002-1656-6362

Junhyoung Lee − *Department of Biological Sciences, Hyupsung University, Hwasung-si 18330, Korea*

Complete contact information is available at: https://pubs.acs.org/10.1021/jacs.1c03875

Author Contributions

J.H.K. and P.V. contributed equally to this work.

Notes

The authors declare no competing financial interest.

■ ACKNOWLEDGMENTS

This work was supported by the Korean Creative Research Initiative (CRI Project No. 2018R1A3B1052702, J.S.K.) and the Basic Science Research Programs (No. 2018R1A2B6002275, J.H.), and the Global PhD Fellowship (GPF) Program (No. 2019H1A2A1074096, J.H.K.) from the National Research Foundation of Korea (NRF) funded by the Korea Ministry of Science and ICT (MSIT). We also gratefully acknowledge support from Korea University and Hyupsung University. Initial support for the work in Austin came from the National Institutes of Health (CA 68682 to J.L.S.) with subsequent funding from the Robert A. Welch Foundation (F-0018 to J.L.S.).

■ REFERENCES

(1) Chow, E. K.-H. Implication of cancer stem cells in cancer drug development and drug delivery. *J. Lab. Autom.* **2013**, *18*, 6−11.

(2) Reya, T.; Morrison, S. J.; Clarke, M. F.; Weissman, I. L. Stem cells, cancer, and cancer stem cells. *Nature* **2001**, *414*, 105−111.

(3) Li, Z.; Rich, J. N. Hypoxia and hypoxia inducible factors in cancer stem cell maintenance. In *Diverse Effects of Hypoxia on Tumor Progression*; Springer: New York, 2010; Vol. *345*, pp 21−30.

(4) Yun, Z.; Lin, Q. Hypoxia and regulation of cancer cell stemness. In *Tumor Microenvironment and Cellular Stress*; Springer: New York, 2014; Vol. *772*, pp 41−53.

(5) Minami, Y. Overview: cancer stem cell and tumor environment. *Oncology* **2015**, *89* (1), 22−24.

(6) Hanahan, D.; Weinberg, R. A. Hallmarks of Cancer: The Next Generation. *Cell* **2011**, *144*, 646−674.

(7) Han, J.; Won, M.; Kim, J. H.; Jung, E.; Min, K.; Jangili, P.; Kim, J. S. Cancer stem cell-targeted bio-imaging and chemotherapeutic perspective. *Chem. Soc. Rev.* **2020**, *49*, 7856−7878.

(8) Yang, L.; Shi, P.; Zhao, G.; Xu, J.; Peng, W.; Zhang, J.; Zhang, G.; Wang, X.; Dong, Z.; Chen, F.; Cui, H. Targeting cancer stem cell pathways for cancer therapy. *Signal Transduct. Target. Ther.* **2020**, *5*, 1−35.

(9) Lee, Y.-A.; Kim, J.-J.; Lee, J.; Lee, J. H. J.; Sahu, S.; Kwon, H. Y.; Park, S.-J.; Jang, S.-Y.; Lee, J.-S.; Wang, Z.; Tam, W. L.; Lim, B.; Kang, N.-Y.; Chang, Y.-T. Identification of tumor initiating cells with a small-molecule fluorescent probe by using vimentin as a biomarker. *Angew. Chem.* **2018**, *130*, 2901−2904.

(10) Kim, J.-J.; Lee, Y.-A.; Su, D.; Lee, J.; Park, S.-J.; Kim, B.; Lee, J. H. J.; Liu, X.; Kim, S. S.; Bae, M. A.; Lee, J.-S.; Hong, S. C.; Wang, L.; Samanta, A.; Kwon, H.-Y.; Choi, S.-Y.; Kim, J.-Y.; Yu, Y. H.; Ha, H.-H.; Wang, Z.; Tam, W. L.; Lim, B.; Kang, N.-Y.; Chang, Y.-T. A Near-Infrared Probe Tracks and Treats Lung Tumor Initiating Cells by Targeting HMOX2. *J. Am. Chem. Soc.* **2019**, *141*, 14673−14686.

(11) Qin, H.; Zhao, C.; Sun, Y.; Ren, J.; Qu, X. Metallo-supramolecular Complexes Enantioselectively Eradicate Cancer Stem Cells in Vivo. *J. Am. Chem. Soc.* **2017**, *139*, 16201−16209.

(12) Li, H.; Yan, W.; Suo, X.; Peng, H.; Yang, X.; Li, Z.; Zhang, J.; Liu, D. Nucleus-targeted nano delivery system eradicates cancer stem cells by combined thermotherapy and hypoxia-activated chemotherapy. *Biomaterials* **2019**, *200*, 1−14.

(13) Debele, T. A.; Yu, L.-Y.; Yang, C.-S.; Shen, Y.-A.; Lo, C.-L. pH- and GSH-sensitive hyaluronic acid-MP conjugate micelles for

intracellular delivery of doxorubicin to colon cancer cells and cancer stem cells. *Biomacromolecules* **2018**, *19*, 3725−3737.

(14) Boodram, J. N.; Mcgregor, I. J.; Bruno, P. M.; Cressey, P. B.; Hemann, M. T.; Suntharalingam, K. Breast Cancer Stem Cell Potent Copper (II)−Non-Steroidal Anti-Inflammatory Drug Complexes. *Angew. Chem.* **2016**, *128*, 2895−2900.

(15) Shen, S.; Xu, X.; Lin, S.; Zhang, Y.; Liu, H.; Zhang, C.; Mo, R. A nanotherapeutic strategy to overcome chemotherapeutic resistance of cancer stem-like cells. *Nat. Nanotechnol.* **2021**, *16*, 104−113.

(16) Muz, B.; de la Puente, P.; Azab, F.; Azab, A. K. J. H. The role of hypoxia in cancer progression, angiogenesis, metastasis, and resistance to therapy. *Hypoxia* **2015**, *3*, 83−92.

(17) Jing, X.; Yang, F.; Shao, C.; Wei, K.; Xie, M.; Shen, H.; Shu, Y. Role of hypoxia in cancer therapy by regulating the tumor microenvironment. *Mol. Cancer* **2019**, *18*, 157.

(18) Zhang, J.; Li, L. Stem cell niche: microenvironment and beyond. *J. Biol. Chem.* **2008**, *283*, 9499−9503.

(19) Brugnoli, F.; Grassilli, S.; Al-Qassab, Y.; Capitani, S.; Bertagnolo, V. CD133 in Breast Cancer Cells: More than a Stem Cell Marker. *J. Oncol.* **2019**, *2019*, 1−8.

(20) Zhang, X.; Zhao, X.; Shao, S.; Zuo, X.; Ning, Q.; Luo, M.; Gu, S.; Zhao, X. Notch1 induces epithelial-mesenchymal transition and the cancer stem cell phenotype in breast cancer cells and STAT3 plays a key role. *Int. J. Oncol.* **2015**, *46*, 1141−1148.

(21) Baker, A.; Wyatt, D.; Bocchetta, M.; Li, J.; Filipovic, A.; Green, A.; Peiffer, D. S.; Fuqua, S.; Miele, L.; Albain, K. S.; Osipo, C. Notch-1-PTEN-ERK1/2 signaling axis promotes HER2+ breast cancer cell proliferation and stem cell survival. *Oncogene* **2018**, *37*, 4489−4504.

(22) Lee, M. H.; Sharma, A.; Chang, M. J.; Lee, J.; Son, S.; Sessler, J. L.; Kang, C.; Kim, J. S. Fluorogenic reaction-based prodrug conjugates as targeted cancer theranostics. *Chem. Soc. Rev.* **2018**, *47*, 28−52.

(23) Sharma, A.; Arambula, J. F.; Koo, S.; Kumar, R.; Singh, H.; Sessler, J. L.; Kim, J. S. Hypoxia-targeted drug delivery. *Chem. Soc. Rev.* **2019**, *48*, 771−813.

(24) O'Connor, L. J.; Cazares-Körner, C.; Saha, J.; Evans, C. N. G.; Stratford, M. R. L.; Hammond, E. M.; Conway, S. J. Design, synthesis and evaluation of molecularly targeted hypoxia-activated prodrugs. *Nat. Protoc.* **2016**, *11*, 781−794.

(25) Winn, B. A.; Shi, Z.; Carlson, G. J.; Wang, Y.; Nguyen, B. L.; Kelly, E. M.; Ross, R. D., IV; Hamel, E.; Chaplin, D. J.; Trawick, M. L.; Pinney, K. G. Bioreductively activatable prodrug conjugates of phenstatin designed to target tumor hypoxia. *Bioorg. Med. Chem. Lett.* **2017**, *27*, 636−641.

(26) Thomson, P.; Naylor, M. A.; Everett, S. A.; Stratford, M. R. L.; Lewis, G.; Hill, S.; Patel, K. B.; Wardman, P.; Davis, P. D. Synthesis and biological properties of bioreductively targeted nitrothienyl prodrugs of combretastatin A-4. *Mol. Cancer Ther.* **2006**, *5*, 2886−2894.

(27) Bruemmer, K. J.; Crossley, S. W. M.; Chang, C. J. Activity-Based Sensing: A Synthetic Methods Approach for Selective Molecular Imaging and Beyond. *Angew. Chem., Int. Ed.* **2020**, *59*, 13734−13762.

(28) Lock, F. E.; McDonald, P. C.; Lou, Y.; Serrano, I.; Chafe, S. C.; Ostlund, C.; Aparicio, S.; Winum, J.-Y.; Supuran, C. T.; Dedhar, S. Targeting carbonic anhydrase IX depletes breast cancer stem cells within the hypoxic niche. *Oncogene* **2013**, *32*, 5210−5219.

(29) Lou, Y.; McDonald, P. C.; Oloumi, A.; Chia, S.; Ostlund, C.; Ahmadi, A.; Kyle, A.; auf dem Keller, U.; Leung, S.; Huntsman, D.; Clarke, B.; Sutherland, B. W.; Waterhouse, D.; Bally, M.; Roskelley, C.; Overall, C. M.; Minchinton, A.; Pacchiano, F.; Carta, F.; Scozzafava, A.; Touisni, N.; Winum, J.-Y.; Supuran, C. T.; Dedhar, S. Targeting tumor hypoxia: suppression of breast tumor growth and metastasis by novel carbonic anhydrase IX inhibitors. *Cancer Res.* **2011**, *71*, 3364−3376.

(30) Tafreshi, N. K.; Lloyd, M. C.; Proemsey, J. B.; Bui, M. M.; Kim, J.; Gillies, R. J.; Morse, D. L. Evaluation of CAIX and CAXII expression in breast cancer at varied O_2 levels: CAIX is the superior surrogate imaging biomarker of tumor hypoxia. *Mol. Imaging Bio.* **2016**, *18*, 219−231.

(31) Petrova, V.; Annicchiarico-Petruzzelli, M.; Melino, G.; Amelio, I. The hypoxic tumour microenvironment. *Oncogenesis* **2018**, *7*, 1−13.

(32) Li, Y.; Zhang, T. Targeting cancer stem cells by curcumin and clinical applications. *Cancer Lett.* **2014**, *346*, 197−205.

(33) Lopresti, A. L. The problem of curcumin and its bioavailability: could its gastrointestinal influence contribute to its overall health-enhancing effects? *Adv. Nutr.* **2018**, *9*, 41−50.

(34) Zaman, M. S.; Chauhan, N.; Yallapu, M. M.; Gara, R. K.; Maher, D. M.; Kumari, S.; Sikander, M.; Khan, S.; Zafar, N.; Jaggi, M.; Chauhan, S. C. Curcumin nanoformulation for cervical cancer treatment. *Sci. Rep.* **2016**, *6*, 20051.

(35) Nelson, K. M.; Dahlin, J. L.; Bisson, J.; Graham, J.; Pauli, G. F.; Walters, M. A. The essential medicinal chemistry of curcumin: miniperspective. *J. Med. Chem.* **2017**, *60*, 1620−1637.

(36) Kanwar, S. S.; Yu, Y.; Nautiyal, J.; Patel, B. B.; Padhye, S.; Sarkar, F. H.; Majumdar, A. P. N. Difluorinated-curcumin (CDF): a novel curcumin analog is a potent inhibitor of colon cancer stem-like cells. *Pharm. Res.* **2011**, *28*, 827−838.

(37) Sahin, K.; Orhan, C.; Tuzcu, M.; Muqbil, I.; Sahin, N.; Gencoglu, H.; Guler, O.; Padhye, S. B.; Sarkar, F. H.; Mohammad, R. M. Comparative in vivo evaluations of curcumin and its analog difluorinated curcumin against cisplatin-induced nephrotoxicity. *Biol. Trace Elem. Res.* **2014**, *157*, 156−163.

(38) Momtazi, A. A.; Sahebkar, A. Difluorinated Curcumin: A Promising Curcumin Analogue with Improved Anti-Tumor Activity and Pharmacokinetic Profile. *Curr. Pharm. Des.* **2016**, *22*, 4386−4397.

(39) Qin, W.; Xu, C.; Zhao, Y.; Yu, C.; Shen, S.; Li, L.; Huang, W. Recent progress in small molecule fluorescent probes for nitroreductase. *Chin. Chem. Lett.* **2018**, *29*, 1451−1455.

(40) Kim, H.; Kim, Y.; Jeoung, D. DDX53 Promotes Cancer Stem Cell-Like Properties and Autophagy. *Mol. Cells* **2017**, *40*, 54−65.

(41) Liu, T. J.; Sun, B. C.; Zhao, X. L.; Zhao, X. M.; Sun, T.; Gu, Q.; Yao, Z.; Dong, X. Y.; Zhao, N.; Liu, N. CD133+ cells with cancer stem cell characteristics associates with vasculogenic mimicry in triple-negative breast cancer. *Oncogene* **2013**, *32*, 544−553.

(42) Jia, Z.; Liang, Y.; Xu, X.; Li, X.; Liu, Q.; Ou, Y.; Duan, L.; Zhu, W.; Lu, W.; Xiong, J.; Wang, D. Isolation and characterization of human mesenchymal stem cells derived from synovial fluid by magnetic-activated cell sorting (MACS). *Cell Biol. Int.* **2018**, *42*, 262−271.

(43) Koo, S.; Bobba, K. N.; Cho, M. Y.; Park, H. S.; Won, M.; Velusamy, N.; Hong, K. S.; Bhuniya, S.; Kim, J. S. Molecular Theranostic Agent with Programmed Activation for Hypoxic Tumors. *ACS Appl. Bio Mater.* **2019**, *2*, 4648−4655.

(44) Kumar, R.; Kim, E.-J.; Han, J.; Lee, H.; Shin, W. S.; Kim, H. M.; Bhuniya, S.; Kim, J. S.; Hong, K. S. Hypoxia-directed and activated theranostic agent: Imaging and treatment of solid tumor. *Biomaterials* **2016**, *104*, 119−128.

(45) Huizing, F. J.; Garousi, J.; Lok, J.; Franssen, G.; Hoeben, B. A. W.; Frejd, F. Y.; Boerman, O. C.; Bussink, J.; Tolmachev, V.; Heskamp, S. CAIX-targeting radiotracers for hypoxia imaging in head and neck cancer models. *Sci. Rep.* **2019**, *9*, 18898.

(46) Robertson, N.; Potter, C.; Harris, A. L. Role of carbonic anhydrase IX in human tumor cell growth, survival, and invasion. *Cancer Res.* **2004**, *64*, 6160−6165.

(47) Marie-Egyptienne, D. T.; Chaudary, N.; Kalliomäki, T.; Hedley, D. W.; Hill, R. P. Cancer initiating-cells are enriched in the CA9 positive fraction of primary cervix cancer xenografts. *Oncotarget* **2017**, *8*, 1392−1404.

(48) Mboge, M. Y.; Chen, Z.; Wolff, A.; Mathias, J. V.; Tu, C.; Brown, K. D.; Bozdag, M.; Carta, F.; Supuran, C. T.; McKenna, R.; Frost, S. C. Selective inhibition of carbonic anhydrase IX over carbonic anhydrase XII in breast cancer cells using benzene sulfonamides: Disconnect between activity and growth inhibition. *PLoS One* **2018**, *13*, e0207417.

(49) Jian, J.; Zhong, N.; Jiang, D.; Li, L.; Lou, Y.; Zhou, W.; Chen, S.; Xiao, J. The embryonic transcription factor Brachyury confers

chordoma chemoresistance via upregulating CA9. *Am. J. Transl. Res.* **2018**, *10*, 936−947.

(50) Nunes, A. S.; Barros, A. S.; Costa, E. C.; Moreira, A. F.; Correia, I. J. 3D tumor spheroids as in vitro models to mimic in vivo human solid tumors resistance to therapeutic drugs. *Biotechnol. Bioeng.* **2019**, *116*, 206−226.

(51) Mimeault, M.; Batra, S. K. Potential applications of curcumin and its novel synthetic analogs and nanotechnology-based formulations in cancer prevention and therapy. *Chin. Med.* **2011**, *6*, 1−19.

(52) Venkatesh, V.; Nataraj, R.; Thangaraj, G. S.; Karthikeyan, M.; Gnanasekaran, A.; Kaginelli, S. B.; Kuppanna, G.; Kallappa, C. G.; Basalingappa, K. M. Targeting Notch signalling pathway of cancer stem cells. *Stem Cell Invest.* **2018**, *5*, 5.

(53) Gruber, W.; Scheidt, T.; Aberger, F.; Huber, C. G. Understanding cell signaling in cancer stem cells for targeted therapy - can phosphoproteomics help to reveal the secrets? *Cell Commun. Signaling* **2017**, *15*, 1−16.

(54) Piva, M.; Domenici, G.; Iriondo, O.; Rábano, M.; Simões, B. M.; Comaills, V.; Barredo, I.; López-Ruiz, J. A.; Zabalza, I.; Kypta, R.; Vivanco, M. D. Sox2 promotes tamoxifen resistance in breast cancer cells. *EMBO Mol. Med.* **2014**, *6*, 66−79.

(55) Domenici, G.; Aurrekoetxea-Rodríguez, I.; Simões, B. M.; Rábano, M.; Lee, S. Y.; Millán, J. S.; Comaills, V.; Oliemuller, E.; López-Ruiz, J. A.; Zabalza, I.; Howard, B. A.; Kypta, R. M.; Vivanco, M. D. A Sox2-Sox9 signalling axis maintains human breast luminal progenitor and breast cancer stem cells. *Oncogene* **2019**, *38*, 3151−3169.

(56) Mukherjee, S.; Mazumdar, M.; Chakraborty, S.; Manna, A.; Saha, S.; Khan, P.; Bhattacharjee, P.; Guha, D.; Adhikary, A.; Mukhjerjee, S.; Das, T. Curcumin inhibits breast cancer stem cell migration by amplifying the E-cadherin/β-catenin negative feedback loop. *Stem Cell Res. Ther.* **2014**, *5*, 116.

(57) Sun, H.-R.; Wang, S.; Yan, S.-C.; Zhang, Y.; Nelson, P. J.; Jia, H.-L.; Qin, L.-X.; Dong, Q.-J. Therapeutic strategies targeting cancer stem cells and their microenvironment. *Front. Oncol.* **2019**, *9*, 1104.

(58) Yoo, D.; Jung, E.; Noh, J.; Hyun, H.; Seon, S.; Hong, S.; Kim, D.; Lee, D. Glutathione-depleting pro-oxidant as a selective anticancer therapeutic agent. *ACS Omega* **2019**, *4*, 10070−10077.

(59) Wang, Y.; Fan, H.; Balakrishnan, K.; Lin, Z.; Cao, S.; Chen, W.; Fan, Y.; Guthrie, Q. A.; Sun, H.; Teske, K. A.; Gandhi, V.; Arnold, L. A.; Peng, X. Hydrogen peroxide activated quinone methide precursors with enhanced DNA cross-linking capability and cytotoxicity towards cancer cells. *Eur. J. Med. Chem.* **2017**, *133*, 197−207.

(60) Sunwoo, K.; Won, M.; Ko, K.-P.; Choi, M.; Arambula, J. F.; Chi, S.-G.; Sessler, J. L.; Verwilst, P.; Kim, J. S. Mitochondrial Relocation of a Common Synthetic Antibiotic: A Non-genotoxic Approach to Cancer Therapy. *Chem.* **2020**, *6*, 1408−1419.

(61) Andergassen, U.; Schlenk, K.; Jeschke, U.; Sommer, H.; Kölbl, A. Epithelial-mesenchymal transition was identified as a potential marker for breast cancer aggressiveness using reverse transcription-quantitative polymerase chain reaction. *Mol. Med. Rep.* **2018**, *18*, 1733−1739.

(62) Kallergi, G.; Papadaki, M. A.; Politaki, E.; Mavroudis, D.; Georgoulias, V.; Agelaki, S. Epithelial to mesenchymal transition markers expressed in circulating tumour cells of early and metastatic breast cancer patients. *Breast Cancer Res.* **2011**, *13*, R59.

(63) Yang, J.; Mani, S. A.; Donaher, J. L.; Ramaswamy, S.; Itzykson, R. A.; Come, C.; Savagner, P.; Gitelman, I.; Richardson, A.; Weinberg, R. A. Twist, a master regulator of morphogenesis, plays an essential role in tumor metastasis. *Cell* **2004**, *117*, 927−939.

(64) Sun, Y.; Song, G. D.; Sun, N.; Chen, J. Q.; Yang, S. S. Slug overexpression induces stemness and promotes hepatocellular carcinoma cell invasion and metastasis. *Oncol. Lett.* **2014**, *7*, 1936−1940.

https://doi.org/10.1021/jacs.1c03875
J. Am. Chem. Soc. XXXX, XXX, XXX−XXX